Elmer Press

Original Article J Neurol Res. 2015;5(1-2):167-180

# A Non-Invasive Detection and Monitoring of Intracranial Pressure Using Ultrasound Sensors

Derek Kwaku Pobi Asiedu[a], Kyoung-Jae Lee[a, b]

## Abstract

**Background:** Intracranial pressure (ICP) measurement is an extremely important part of the neurosurgical healthcare. Existing methods used for monitoring ICP are mainly grouped into invasive and non-invasive methods. Research into techniques for ICP monitoring is now gearing towards non-invasive methods to eliminate complications associated with invasive methods. The goal of this work was to propose an effective method for ICP monitoring.

**Method:** The work presents a model-based approach for the analysis and characterization of the proposed method. ICP waveforms and characteristics were generated from mathematical models using computer simulation and various datasets. The simulation model of the proposed ultrasound system and biological system were developed.

**Results:** The ICP pulse was achieved with a variance of 63.62 Pa from the reference model used. From our results, a minimum of 10 MHz with a minimum pulse width of 80 µs can be used in the development of proposed system. The cut-off frequencies for the pulse generator filter and mixed signal filter values were 40 MHz and 1 MHz respectively.

**Conclusion:** The present study establishes a reference model for ultrasound system-biological system interaction. The study also proposes a new approach for ICP monitoring. The ICP monitoring approach in this paper has the advantage of being a simple, non-invasive and a direct method for ICP monitoring. The model presented is an effective tool in the field of research, coursework and presentations. The introduced device satisfies both the needs of the patients and that of the health personnel.

**Keywords:** Intracranial pressure; Non-invasive; Monitoring; Ultrasound technique; Human neck region

Manuscript accepted for publication February 23, 2015

[a]Department of Electronics and Control Engineering, College of Information Technology, Hanbat National University, Daejeon, Korea
[b]Corresponding Author: Kyoung-Jae Lee, Department of Electronics and Control Engineering, College of Information Technology, Hanbat National University, Daejeon, Korea. Email: kyoungjae@hanbat.ac.kr

doi: http://dx.doi.org/10.14740/jnr322w

## Introduction

Intracranial pressure (ICP) is termed as the pressure found within the skull due to the presence of the cerebrospinal fluid (CSF) [1]. ICP waveform consists of three main peaks. These three peaks as seen in Figure 1 are the percussion wave (P1: represents arterial pulsation), tidal wave (P2: represents intracranial compliance) and dicrotic wave (P3: represents aortic valve closure). For normal ICP waveform, P1 has the highest value and P3 the lowest. P2 is higher than P1 in an abnormal ICP wave (i.e. increased ICP) [2, 3]. The increase in ICP can be either acute or chronic. The increase in ICP may be caused by intracranial tumors, blood vessel anomalies and infections [1]. Increased ICP can lead to death and devastating neurological damage [4]. ICP monitoring is therefore important in neurological healthcare [4]. Clinical ICP monitoring can be grouped into two methods, namely invasive methods (penetrating the human body) and non-invasive methods (no penetration of the human body) [4]. Current ICP monitoring research is geared towards non-invasive techniques [5]. This is to help eliminate problems associated with invasive methods of ICP monitoring [4-6]. The problems associated with invasive ICP monitoring can be categorized into complications (blood clots, air bubbles, etc.), infections, discomfort, obstructions, hemorrhages and ICP value inaccuracy (with some invasive methods) [4, 6].

Various non-invasive ICP monitoring methods researched have shown promise in eliminating the problems associated with their invasive counterparts. Current research of various non-invasive ICP monitoring methods can be found in the reviews of Wayne et al, Jackrit et al, Newman et al, Noble et al and Derek et al [6-10]. The use of existing non-invasive medical diagnosis equipment, the development of new devices based on medical theories and the use of computational

**Figure 1.** Proposed model for ICP monitoring device.

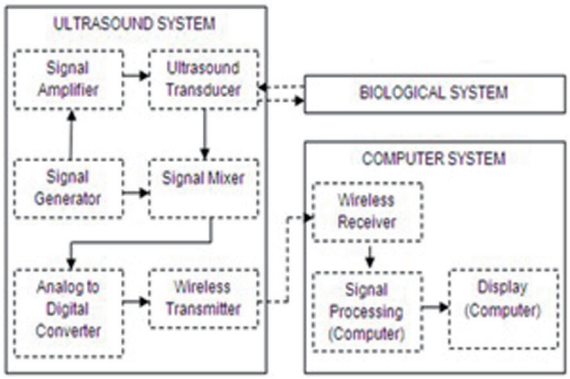


**Figure 2.** Proposed ICP monitoring device system components breakdown.

methods are some of the current techniques being researched on [7-10]. Present non-invasive methods for monitoring ICP reviewed achieve their main purpose of eliminating the need for invasion of the human body but also present their associated disadvantages. Inaccuracy, patient specific monitoring devices, lack of real-time monitoring, patient complication and poor theoretical framework are some of the problems associated with these current methods of non-invasive ICP monitoring [8].

The identification of better non-invasive ICP measuring method will go a long way to help improve neurological healthcare, reduce deaths from poor diagnosis of ICP, and introduce a less painful, safe and reliable ICP measuring device into neurological healthcare. This paper focuses on presenting a new approach (method) for ICP monitoring from the posterior end of the human neck region using an ultrasound sensor. The choice of design is to solve problems associated with current ICP monitoring stated in the previous section (introduction). Furthermore this design allows patient mobility within a specific range (wireless transmission range), allows bedside monitoring and can be used on a wide range of patients. This system will also reduce bulkiness around patient rooms (e.g. ICUs) and allow easy operation by healthcare persons. The work presented also pursues a unified analytical study of the human biology-proposed ICP monitoring method interaction. The significant contribution of this work is emphasized by its uniqueness and the success in conducting simulations that have answered the concerns relevant to the proposed ICP monitoring technique.

### System model

The concept for the proposed ICP monitoring device can be seen in Figure 1; the ultrasound sensor system will be attached to posterior end of the human neck region (i.e. between base of skull and C2). The detected signals will then be transmitted wirelessly to the computing system for signal processing to acquire ICP waveform of the patient. The boxes in Figure 2 represent functions performed by the computer and other electronic circuits and not individual physical components [11-15]. The assumptions and considerations made for the biological system were to reduce complexity and focus solely on establishing the proposed theory. It is assumed in this research that the neck region from the posterior end consists of lumped sub-regions of the skin, muscle, mater and the spinal cord. For Doppler effect, it is assumed the ultrasound reflections analyzed are from cells within the CSF. Note also that physical structures of tissues and organs beyond the cervical column and its content were not considered in this research.

Ultrasound pulses used for the acquisition of phase shift values were acquired by modifying a mathematical model of biological signals to acquire the tri-phasic structure of ICP [16, 17]. The theoretical framework for the ultrasound propagation consists of basic ultrasound theory and the Doppler theory. When ultrasound pulses are transmitted into a body several things happen when [12, 13] most of the ultrasound energy is absorbed and the beam is attenuated (these are undesirable and do not contribute to diagnosis), some of the pulses will be reflected by internal body structures and these echoes return to the surface where they are collected by the ultrasound transducer for diagnosis. The equations used to characterize the behavior of ICP, ultrasound pulses and Doppler theory can be found in references [11-13, 16, 17]. Mathematical equation for ICP tri-phasic pulse generation is: $ICP = \mu_o + [\mu_1 \cos(2\pi f_c t)] + [\mu_2 \cos(4\pi f_c t + \theta)] + [\mu_3 \cos(4\pi f_c t + \theta)]$.

## Methodology

The methodology for this research can be split into two main parts. These are the biological system and ultrasound interaction, and the device functionality. The biological system-ultrasound interaction concentrates on finding the appropriate ultrasound frequencies and transmission mode to use, the behavior of ultrasound within the chosen biological region and the effects of the ultrasound on the various tissues. The device functionality concentrated on understanding the basic components needed in specifications and development of the ICP monitoring device. The SIMULINK model developed was a variation of Bjorsell et al [18] and Hillard et al [19].

### Biological system-ultrasound interaction

Table 1 shows a list of neck region tissues considered in this simulation, their thickness (dimension) and their ultrasonic properties [20-27]. The extreme values acquired for this work were from infants (1 - 6 years) and adults (34 years). Ten datasets were generated from these intervals and used for research analysis (Table 2). In this research pulsed ultrasound signal transmission was used. Continuous ultrasound transmission was not used because of possibility of standing waves and possible continuous heating within biological tissues considered [28].

The appropriate ultrasound frequency/frequencies for transmission within individuals/across ages were the initial step taken. From the appropriate frequencies, the best and

**Table 1.** Properties of Various Tissue Regions Used in MATLAB Simulation of Ultrasound Propagation Within the Neck Region

| Regions | Properties | | | |
|---|---|---|---|---|
| | Density (kg/m$^3$) | Speed of sound (m/s) | Attenuation (Np/m/MHz) | Tissue thickness (mm) |
| Transducer | 7,660 | 5200 | - | - |
| Skin | 1,010 - 1,020 | 1,720 - 1,540 | 3.300 | 1.4 - 4 |
| Neck muscle | 1,040 - 1,070 | 1,580 - 1,566 | 20.000 | 14 - 27.5, 10 - 14.5 |
| Vertebra column | 1,400 - 1,810 | 3,299 - 4,080 | 1.000 | 10 - 13.0 |
| Dura mater | 1,010 - 1,020 | 1,720 - 1,540 | 0.025 | 0.4 - 0.9 |
| Cerebrospinal fluid | 990 - 1,000 | 1,527 - 1,519 | 1.000 | 0.3 - 0.5 |
| Spinal cord | 1,010 - 1,020 | 1,720 - 1,540 | 0.025 | 2 - 3.51 |

minimum frequency which can be used across was selected. The frequency/frequencies selected were used to identify the amplitudes and signal detection time for the various tissues considered. The position/point of contact on the neck region (i.e. between base of skull and C7) [29] was also selected using MATLAB simulations of ultrasound propagation within the neck region. The position was identified using the amplitude of ultrasound signal received. These analyses were performed using the ultrasound characterization equations [11, 13, 15, 20]. Also, the model considered scenarios within the neck region where vertebra column was present and not present. The ultrasound transducer diameter used in this work was 2 mm.

### Ultrasound device characterization

SIMULINK was used for the characterization and understanding of the various components for the proposed ICP monitoring device (i.e. in Fig. 1, 2).The ultrasound transducer circuit represents the receiver circuit attached to the neck region.

**Table 2.** Dataset Generated Table From Initial Parameters

| Region | Range | | | | | | | | | |
|---|---|---|---|---|---|---|---|---|---|---|
| | 1 | 2 | 3 | 4 | 5 | 6 | 7 | 8 | 9 | 10 |
| Density (kg/m$^3$) | | | | | | | | | | |
| Skin | 1,010 | 1,011 | 1,012 | 1,013 | 1,014 | 1,015 | 1,016 | 1,017 | 1,018 | 1,020 |
| Muscle | 1,040 | 1,043 | 1,046 | 1,050 | 1,053 | 1,056 | 1,060 | 1,063 | 1,066 | 1,070 |
| Vertebra | 1,400 | 1,445 | 1,491 | 1,536 | 1,582 | 1,627 | 1,673 | 1,718 | 1,764 | 1,810 |
| Dura | 1,010 | 1,011 | 1,012 | 1,013 | 1,014 | 1,015 | 1,016 | 1,017 | 1,018 | 1,020 |
| CSF | 990 | 991 | 992 | 993 | 994 | 995 | 996 | 997 | 998 | 1,000 |
| Spine | 1,010 | 1,011 | 1,012 | 1,013 | 1,014 | 1,015 | 1,016 | 1,017 | 1,018 | 1,020 |
| Speed of sound (m/s) | | | | | | | | | | |
| Skin | 1,720 | 1,700 | 1,680 | 1,660 | 1,640 | 1,620 | 1,600 | 1,580 | 1,560 | 1,540 |
| Muscle | 1,580 | 1,578 | 1,577 | 1,575 | 1,574 | 1,572 | 1,571 | 1,569 | 1,568 | 1,566 |
| Vertebra | 3,299 | 3,386 | 3,472 | 3,559 | 3,646 | 3,733 | 3,820 | 3,906 | 3,993 | 4,080 |
| Dura | 1,720 | 1,700 | 1,680 | 1,660 | 1,640 | 1,620 | 1,600 | 1,580 | 1,560 | 1,540 |
| CSF | 1,527 | 1,526 | 1,525 | 1,524 | 1,523.4 | 1,523 | 1,522 | 1,521 | 1,520 | 1,519 |
| Spine | 1,720 | 1,700 | 1,680 | 1,660 | 1,640 | 1,620 | 1,600 | 1,580 | 1,560 | 1,540 |
| Thickness (mm) | | | | | | | | | | |
| Skin | 1.40 | 1.70 | 2.00 | 2.30 | 2.60 | 2.80 | 3.10 | 3.40 | 3.70 | 4.00 |
| Muscle | 27.50, 14.50 | 26.00, 14.00 | 24.50, 13.50 | 23.00, 13.00 | 21.50, 12.50 | 20.00, 12.00 | 18.50, 11.50 | 17.00, 11.00 | 15.50, 10.50 | 14.00, 10.00 |
| Vertebra | 10.00 | 10.30 | 10.70 | 11.00 | 11.30 | 11.70 | 12.00 | 12.30 | 12.70 | 13.00 |
| Dura | 0.40 | 0.46 | 0.51 | 0.57 | 0.62 | 0.70 | 0.73 | 0.80 | 0.84 | 0.90 |
| CSF | 0.30 | 0.32 | 0.34 | 0.37 | 0.39 | 0.41 | 0.43 | 0.45 | 0.48 | 0.50 |
| Spine | 2.00 | 2.20 | 2.30 | 2.50 | 2.70 | 2.80 | 3.00 | 3.20 | 3.30 | 3.50 |

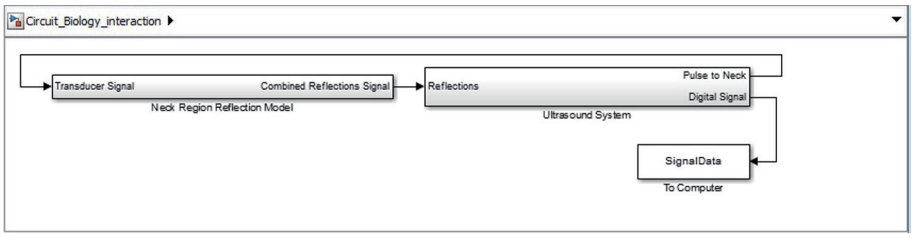


**Figure 3.** SIMULINK model of biological system-ultrasound device interaction.

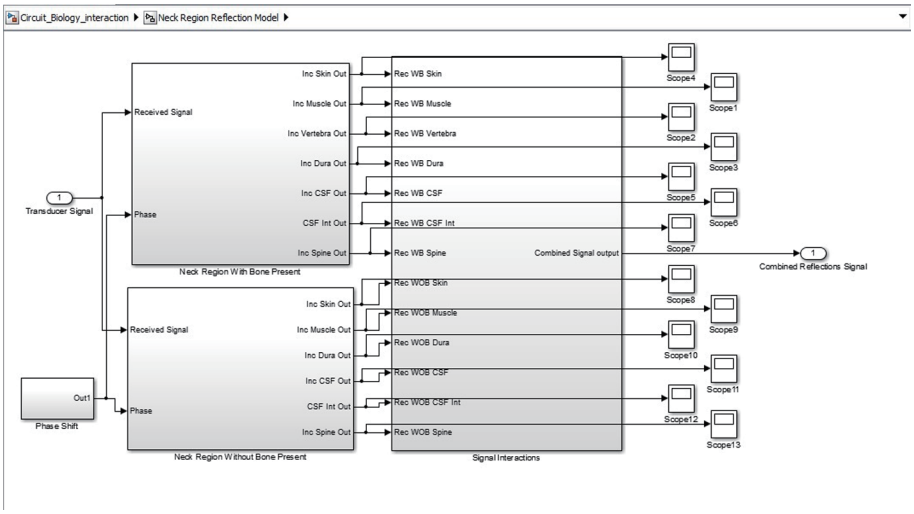


**Figure 4.** Biological system SIMULINK model.

The sub-systems/ components of the transducer receiver were modeled using different specifications to acquire the best option. The model of wireless transfer was not included in this study but may be considered for further research work. The computer system represents the wireless signal receiver and processor. For the computer system, spectral analysis to acquire the fundamental shift frequency was performed. From the frequency the velocity of CSF was calculated which was used to acquire the pressure (ICP) value using the Doppler theory equations and Bernoulli equation. The various main device components developed in SIMULINK can be seen in Figures 3-5. The subcomponents of the device Simulink model can be found in Figures 6-13.

## Results and Discussions

### Biological system-ultrasound interaction

From the procedures discussed in Results section, we first need to identify the various ultrasound propagation characteristics needed to be considered in the device design. Table 3 shows the depth of penetration of ultrasound waves with their corresponding frequencies for the various 10 sets of data generated. From Table 3, Figure 14 was acquired. Figure 14 shows the appropriate ultrasound frequencies for each tissue penetration in each dataset. From the figure, we notice that as the tissue

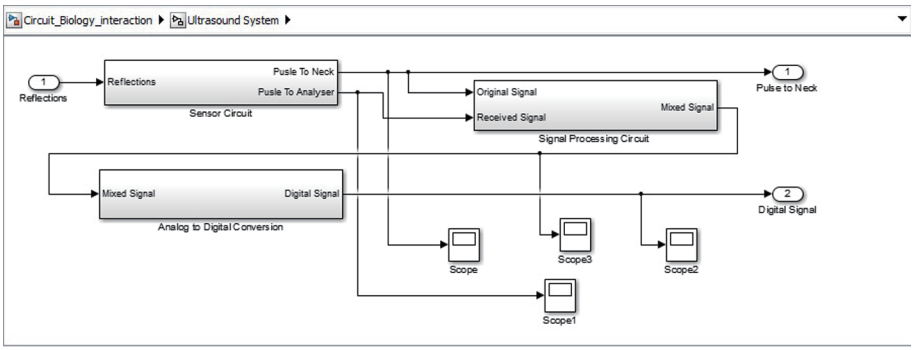


**Figure 5.** Ultrasound system SIMULINK model.

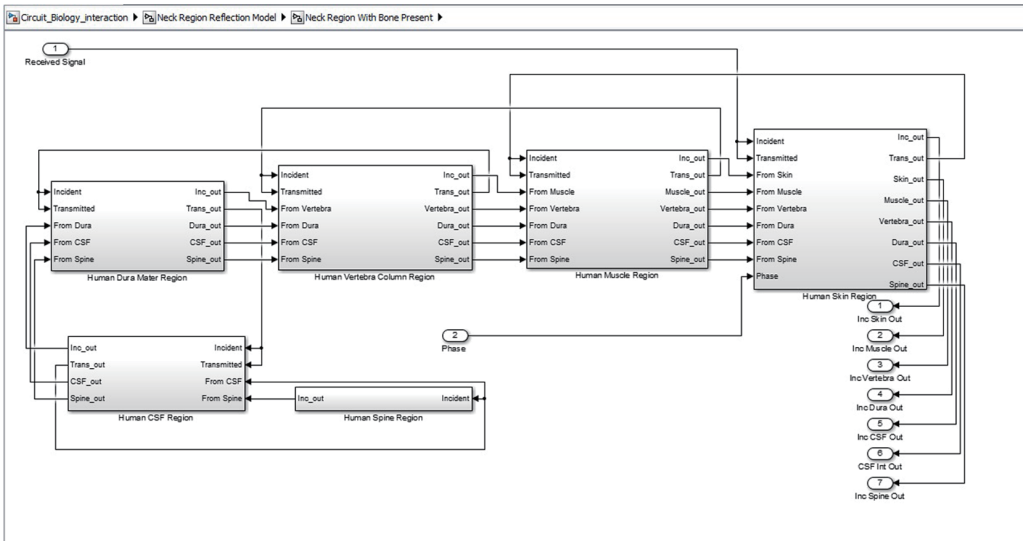


**Figure 6.** Inner structure of neck region showing various tissue levels.

sizes increase in the dataset the frequency needed for penetration of the tissues may increase (i.e. as seen for vertebra and muscle regions). From this result, a minimum of 10 MHz and a maximum of 15 MHz ultrasound frequency can be used for the proposed device. The minimum frequency can be used on individuals with thinner tissue thickness (e.g. infants) while the maximum value can be used on individuals with larger tissue thickness (e.g. adults).

The "time of travel" for ultrasound signal from and to the posterior surface of the neck region was then calculated using MATLAB simulations. This can be found in Table 4. The graph in Figure 15 also shows a representation of these various times of travel for the various datasets created. From this dataset, the minimum time interval between transmission and receiving the ultrasound pulse should be 40 μs. But for a safer and more robust system, twice the interval time should be used. This is to cater for variations between physical human neck tissues of patients. The ICP pulse from literature has a fundamental frequency between 1 Hz and 2 Hz [16, 17]. For the Nyquist criteria a minimum of 4 Hz is need as sampling frequency. But

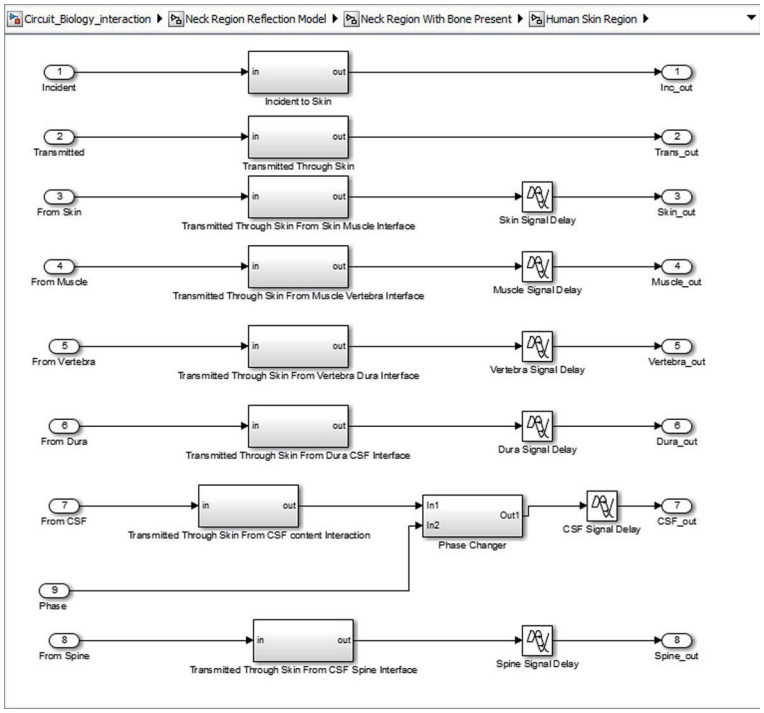


**Figure 7.** Sub-structure for each neck region tissue.

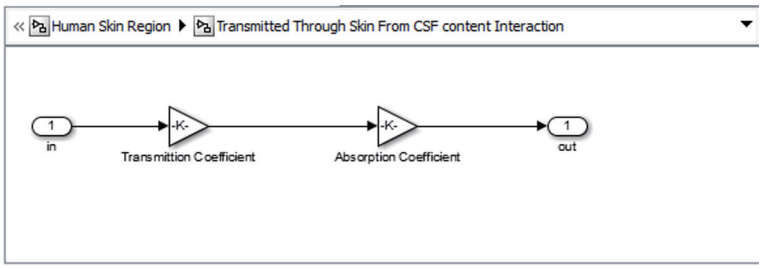


**Figure 8.** Basic unit for representing each tissue.

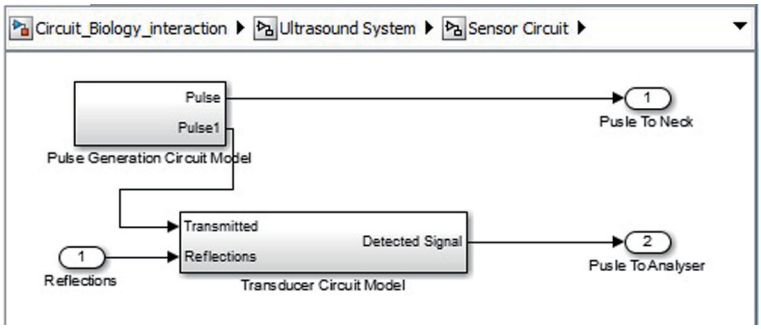


**Figure 9.** Ultrasound system sensor circuit inner structure.

with the 80 µs, ICP pulse is sampled at a frequency of 0.125 MHz (125,000 Hz).

The final consideration for ultrasound propagation was the amplitudes of the ultrasound received pulse. This was to help identify the amount of amplification need before the received ultrasound signal processing is done. A maximum of 15 V intensity was used in this part of the research simulation. Figure 16 shows the various amplitudes of ultrasound signal from each test set. The amplitudes plotted in the Figure 16 below are assumed to be the average amplitudes received from CSF con-

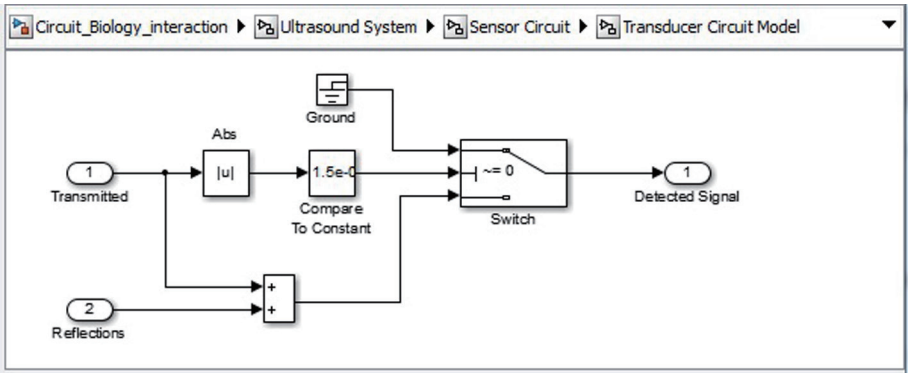


**Figure 10.** Ultrasound system sensor circuit transducer circuit.

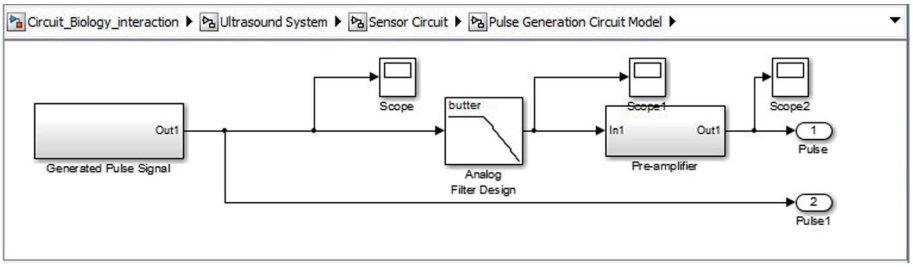


**Figure 11.** Signal generation SIMULINK model.

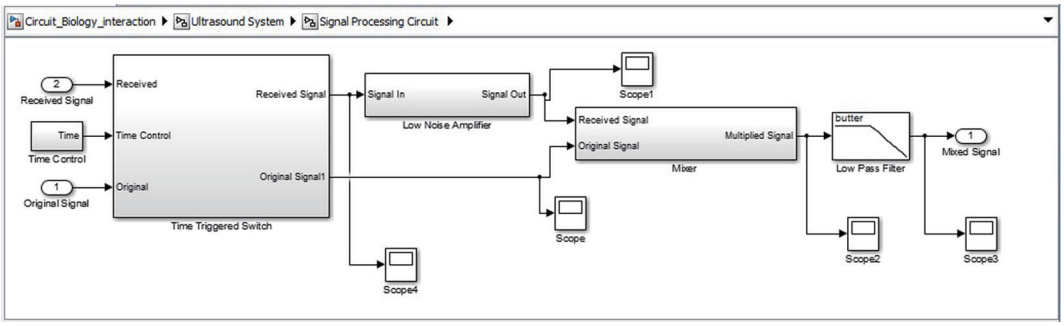


**Figure 12.** Signal processing circuit SIMULINK model.

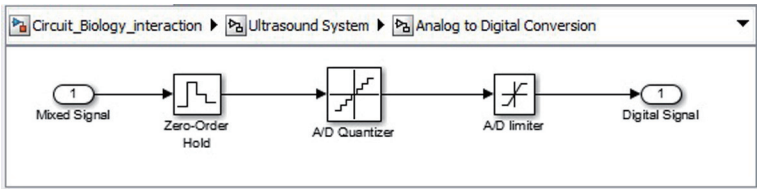


**Figure 13.** Analogue to digital convertor circuit.

**Table 3.** Fresnel Length for a Range of Speed of Sound for Various Tissue Regions

| Speed of sound (m/s) | Fresnel length (mm) | | | | | | | | | Region thickness (mm) |
|---|---|---|---|---|---|---|---|---|---|---|
| | 2 MHz | 3 MHz | 5 MHz | 8 MHz | 10 MHz | 12 MHz | 15 MHz | 18 MHz | 20 MHz | |
| Skin region | | | | | | | | | | |
| 1,720 | 4.651 | 6.976 | 11.627 | 18.604 | 23.255 | 27.906 | 34.882 | 41.860 | 46.511 | 1.40 |
| 1,700 | 4.705 | 7.058 | 11.764 | 18.823 | 23.529 | 28.235 | 35.294 | 42.352 | 47.058 | 1.70 |
| 1,680 | 4.761 | 7.142 | 11.904 | 19.047 | 23.809 | 28.571 | 35.714 | 42.857 | 47.619 | 2.00 |
| 1,660 | 4.819 | 7.228 | 12.048 | 19.277 | 24.390 | 28.915 | 36.144 | 43.373 | 48.192 | 2.30 |
| 1,640 | 4.878 | 7.317 | 12.195 | 19.512 | 24.391 | 29.268 | 36.585 | 43.902 | 48.780 | 2.60 |
| 1,620 | 4.938 | 7.407 | 12.345 | 19.753 | 24.691 | 29.629 | 37.037 | 44.444 | 49.382 | 2.80 |
| 1,600 | 5.000 | 7.500 | 12.500 | 20.000 | 25.000 | 30.000 | 37.500 | 45.000 | 50.000 | 3.10 |
| 1,580 | 5.063 | 7.594 | 12.658 | 20.253 | 25.316 | 30.379 | 37.974 | 45.569 | 50.632 | 3.40 |
| 1,560 | 5.128 | 7.692 | 12.820 | 20.512 | 25.641 | 30.769 | 38.461 | 46.153 | 51.282 | 3.70 |
| 1,540 | 5.194 | 7.792 | 12.987 | 20.779 | 25.974 | 31.168 | 38.961 | 46.753 | 51.948 | 4.00 |
| Muscle region | | | | | | | | | | |
| 1,580 | 5.063 | 7.594 | 12.658 | 20.253 | 25.316 | 30.379 | 37.974 | 45.569 | 50.632 | 14.0, 10.0 |
| 1,578 | 5.068 | 7.602 | 12.670 | 20.273 | 25.341 | 30.409 | 38.012 | 45.614 | 50.682 | 15.5, 10.5 |
| 1,577 | 5.073 | 7.609 | 12.683 | 20.293 | 25.366 | 30.439 | 38.049 | 45.659 | 50.732 | 17.0, 11.0 |
| 1,575 | 5.078 | 7.617 | 12.695 | 20.313 | 25.391 | 30.469 | 30.087 | 45.704 | 50.782 | 18.5, 11.5 |
| 1,574 | 5.083 | 7.624 | 12.708 | 20.333 | 25.416 | 30.499 | 38.124 | 45.749 | 50.833 | 20.0, 12.0 |
| 1,572 | 5.088 | 7.632 | 12.720 | 20.353 | 25.441 | 30.530 | 38.162 | 45.795 | 50.883 | 21.5, 12.5 |
| 1,571 | 5.093 | 7.640 | 12.733 | 20.373 | 25.466 | 30.560 | 38.200 | 45.840 | 50.933 | 23.0, 13.0 |
| 1,569 | 5.098 | 7.647 | 12.746 | 20.393 | 25.492 | 30.590 | 38.238 | 45.885 | 50.984 | 24.5, 13.5 |
| 1,568 | 5.103 | 7.655 | 12.758 | 20.413 | 25.517 | 30.620 | 38.276 | 45.931 | 51.034 | 26.0, 14.0 |
| 1,566 | 5.108 | 7.662 | 12.771 | 20,434 | 25,542 | 30.651 | 38.314 | 45.977 | 51.085 | 27.5, 14.5 |
| Vertebra region | | | | | | | | | | |
| 3,299 | 2.424 | 3.637 | 6.062 | 9.699 | 12.124 | 14.559 | 18.187 | 21.824 | 24.249 | 10.0 |

**Table 3.** Fresnel Length for a Range of Speed of Sound for Various Tissue Regions - *(Continued)*

| Speed of sound (m/s) | Fresnel length (mm) | | | | | | | | | Region thickness (mm) |
|---|---|---|---|---|---|---|---|---|---|---|
| | 2 MHz | 3 MHz | 5 MHz | 8 MHz | 10 MHz | 12 MHz | 15 MHz | 18 MHz | 20 MHz | |
| 3,386 | 2.362 | 3.544 | 5.907 | 9.451 | 11.814 | 14.176 | 17.721 | 21.265 | 23.628 | 10.3 |
| 3,472 | 2.303 | 3.455 | 5.759 | 9.215 | 11.518 | 13.822 | 17.278 | 20.734 | 23.037 | 10.7 |
| 3,559 | 2.247 | 3.371 | 5.619 | 8.990 | 11.238 | 13.485 | 16.875 | 20.228 | 22.476 | 11.0 |
| 3,646 | 2.194 | 3.291 | 5.485 | 8.776 | 10.970 | 13.164 | 16.455 | 19.747 | 21.941 | 11.3 |
| 3,733 | 2.143 | 3.214 | 5.357 | 8.572 | 10.715 | 12.858 | 16.073 | 19.288 | 21.431 | 11.7 |
| 3,820 | 2.094 | 3.141 | 5.236 | 8.377 | 10.472 | 12.566 | 15.708 | 18.849 | 20.944 | 12.0 |
| 3,906 | 2.047 | 3.071 | 5.119 | 8.191 | 10.239 | 12.287 | 17.359 | 18.431 | 20.478 | 12.3 |
| 3,993 | 2.003 | 3.005 | 5.008 | 8.013 | 10.016 | 12.020 | 15.025 | 18.030 | 20.033 | 12.7 |
| 4,080 | 1.960 | 2.941 | 4.901 | 7.843 | 9.803 | 11.764 | 14.705 | 17.647 | 19.607 | 13.0 |
| Dura region | | | | | | | | | | |
| 1,720 | 4.651 | 6.976 | 11.627 | 18.604 | 23.255 | 27.906 | 34.882 | 41.860 | 46.511 | 0.40 |
| 1,700 | 4.705 | 7.058 | 11.764 | 18.823 | 23.529 | 28.235 | 35.294 | 42.352 | 47.058 | 0.46 |
| 1,680 | 4.761 | 7.142 | 11.904 | 19.047 | 23.809 | 28.571 | 35.714 | 42.857 | 47.619 | 0.51 |
| 1,660 | 4.819 | 7.228 | 12.048 | 19.277 | 24.390 | 28.915 | 36.144 | 43.373 | 48.192 | 0.57 |
| 1,640 | 4.878 | 7.317 | 12.195 | 19.512 | 24.391 | 29.268 | 36.585 | 43.902 | 48.780 | 0.62 |
| 1,620 | 4.938 | 7.407 | 12.345 | 19.753 | 24.691 | 29.629 | 37.037 | 44.444 | 49.382 | 0.70 |
| 1,600 | 5.000 | 7.500 | 12.500 | 20.000 | 25.000 | 30.000 | 37.500 | 45.000 | 50.000 | 0.73 |
| 1,580 | 5.063 | 7.594 | 12.658 | 20.253 | 25.316 | 30.379 | 37.974 | 45.569 | 50.632 | 0.80 |
| 1,560 | 5.128 | 7.692 | 12.820 | 20.512 | 25.641 | 30.769 | 38.461 | 46.153 | 51.282 | 0.84 |
| 1,540 | 5.194 | 7.792 | 12.987 | 20.779 | 25.974 | 31.168 | 38.961 | 46.753 | 51.948 | 0.90 |
| CSF region | | | | | | | | | | |
| 1,527 | 5.239 | 7.858 | 13.097 | 20.956 | 26.195 | 31.434 | 39.292 | 47.151 | 52.390 | 0.30 |
| 1,526 | 5.242 | 7.863 | 13.105 | 20.968 | 26.210 | 31.452 | 39.315 | 47.187 | 52.420 | 0.32 |
| 1,525 | 5.245 | 7.867 | 13.112 | 20.980 | 26.225 | 31.470 | 39.338 | 47.206 | 52.451 | 0.34 |
| 1,524 | 5.248 | 7.872 | 13.120 | 20.992 | 26.240 | 31.489 | 39.631 | 47.233 | 52.481 | 0.37 |
| 1,523.4 | 5.251 | 7.876 | 13.128 | 21.005 | 26.256 | 31.507 | 39.384 | 47.261 | 52.512 | 0.39 |
| 1,523 | 5.254 | 7.881 | 13.135 | 21.017 | 26.271 | 31.525 | 39.407 | 47.288 | 52.543 | 0.41 |
| 1,522 | 5.257 | 7.886 | 13.143 | 21.029 | 26.286 | 31.544 | 39.430 | 47.316 | 52,573 | 0.43 |
| 1,521 | 5.260 | 7.890 | 13.151 | 21.041 | 26.302 | 31.562 | 39.453 | 47.344 | 52.604 | 0.45 |
| 1,520 | 5.263 | 7.895 | 13.158 | 21.054 | 26.317 | 31.581 | 39.476 | 47.371 | 52.635 | 0.48 |
| 1,519 | 5.266 | 7.899 | 13.166 | 21.066 | 26.333 | 31.599 | 39.499 | 47.399 | 52.666 | 0.50 |
| Spinal region | | | | | | | | | | |
| 1,720 | 4.651 | 6.976 | 11.627 | 18.604 | 23.255 | 27.906 | 34.882 | 41.860 | 46.511 | 2.00 |
| 1,700 | 4.705 | 7.058 | 11.764 | 18.823 | 23.529 | 28.235 | 35.294 | 42.352 | 47.058 | 2.20 |
| 1,680 | 4.761 | 7.142 | 11.904 | 19.047 | 23.809 | 28.571 | 35.714 | 42.857 | 47.619 | 2.30 |
| 1,660 | 4.819 | 7.228 | 12.048 | 19.277 | 24.390 | 28.915 | 36.144 | 43.373 | 48.192 | 2.50 |
| 1,640 | 4.878 | 7.317 | 12.195 | 19.512 | 24.391 | 29.268 | 36.585 | 43.902 | 48.780 | 2.70 |
| 1,620 | 4.938 | 7.407 | 12.345 | 19.753 | 24.691 | 29.629 | 37.037 | 44.444 | 49.382 | 2.80 |
| 1,600 | 5.000 | 7.500 | 12.500 | 20.000 | 25.000 | 30.000 | 37.500 | 45.000 | 50.000 | 3.00 |
| 1,580 | 5.063 | 7.594 | 12.658 | 20.253 | 25.316 | 30.379 | 37.974 | 45.569 | 50.632 | 3.20 |
| 1,560 | 5.128 | 7.692 | 12.820 | 20.512 | 25.641 | 30.769 | 38.461 | 46.153 | 51.282 | 3.30 |
| 1,540 | 5.194 | 7.792 | 12.987 | 20.779 | 25.974 | 31.168 | 38.961 | 46.753 | 51.948 | 3.50 |

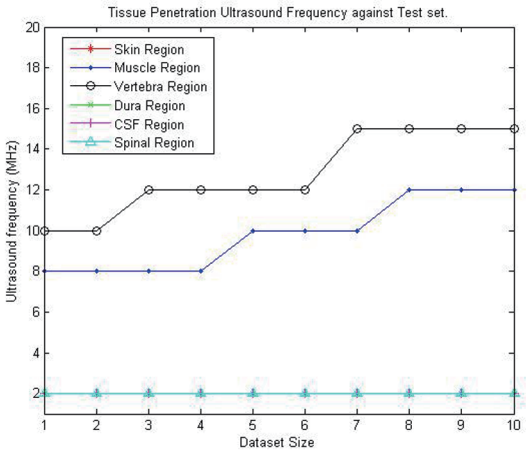


**Figure 14.** Graphical representation of appropriate ultrasound penetration frequencies for each dataset.

tents reflecting ultrasound signal. From the figure, we can also notice that the best position for detecting ultrasound pulses is where there are no bones present. Therefore, the ultrasound sensor can be placed between the base of the skull and C2 to acquire high received ultrasound amplitudes to be processed.

### Ultrasound device characterization

The results acquired from the biological system were used in the modeling of the ultrasound system. The phase shift due to CSF cells and ultrasound signal were acquired from the ICP mathematical model values. The coefficient values for reflection and transmission were used to model the biological tissues (Table 4). For a constant cut of frequency in the pulse generator design, a 40 MHz cut-off frequency for a low pass filter was used. The initial pulse generated was 5 V with a preamplifier with gain 3. A fixed cut-off frequency for the multiplexed ultrasound transmitted and received signal was needed. From Figure 17 and the use of MATLAB FFT function, the cut-off

**Table 4.** Ultrasound Characteristics for Various Tissue Lengths From Simulation

| Region thickness (mm) | Wavelength (mm) | Travel time (µs) | | Attenuation (Gain) | | Coefficients | | | |
|---|---|---|---|---|---|---|---|---|---|
| | | | | | | Reflection | | Transmission | |
| | | A | B | A | B | A | B | A | B |
| Test set 1 - 10 MHz | | | | | | | | | |
| 1.40 | 0.1720 | 0.81 | 0.81 | 0.9999 | 0.9999 | 0.8398 | 0.8398 | 0.1602 | 0.1602 |
| 14.0, 10.0 | 0.1580 | 8.90 | 17.33 | 0.9935 | 0.9967 | 0.0008 | 0.0008 | 0.9999 | 0.9992 |
| 10.0 | 0.3299 | 3.03 | - | 0.9801 | - | 0.2257 | - | 0.7742 | - |
| 0.40 | 0.1720 | 0.23 | 0.23 | 0.9999 | 0.9999 | 0.2055 | 0.2055 | 0.7945 | 0.7945 |
| 0.30 | 0.1527 | 0.20 | 0.20 | 0.9999 | 0.9999 | 0.0048 | 0.0048 | 0.9952 | 0.9952 |
| 2.00 | 0.1720 | 1.20 | 1.20 | 0.9999 | 0.9999 | 0.0048 | 0.0048 | 0.9952 | 0.9952 |
| Test set 2 - 10 MHz | | | | | | | | | |
| 1.70 | 0.1700 | 1.00 | 1.00 | 0.9999 | 0.9999 | 0.8400 | 0.8400 | 0.1600 | 0.1600 |
| 15.5, 10.5 | 0.1578 | 8.87 | 16.5 | 0.9936 | 0.9779 | 0.0005 | 0.0005 | 0.9995 | 0.9995 |
| 10.3 | 0.3386 | 3.04 | - | 0.9790 | - | 0.2466 | - | 0.7534 | - |
| 0.46 | 0.1700 | 0.27 | 0.27 | 0.9999 | 0.9999 | 0.3145 | 0.3145 | 0.6855 | 0.6854 |
| 0.32 | 0.1526 | 0.21 | 0.21 | 0.9999 | 0.9999 | 0.7056 | 0.7056 | 0.2944 | 0.2944 |
| 2.20 | 0.1700 | 1.29 | 1.29 | 0.9999 | 0.9999 | 0.0041 | 0.0041 | 0.9959 | 0.9959 |
| Test set 3 - 12 MHz | | | | | | | | | |
| 2.00 | 0.1680 | 1.20 | 1.20 | 0.9999 | 0.9999 | 0.8430 | 0.8430 | 0.1570 | 0.1570 |
| 17.0, 11.0 | 0.1577 | 8.56 | 15.53 | 0.9765 | 0.9765 | 0.0002 | 0.0002 | 0.9998 | 0.9998 |
| 10.7 | 0.3472 | 3.08 | - | 0.9730 | - | 0.2670 | - | 0.7330 | - |
| 0.51 | 0.1640 | 0.30 | 0.30 | 0.9999 | 0.9999 | 0.2556 | 0.0002 | 0.7444 | 0.9998 |
| 0.34 | 0.1525 | 0.23 | 0.23 | 0.9999 | 0.9999 | 0.0034 | 0.0034 | 0.9966 | 0.9966 |
| 2.30 | 0.1700 | 1.37 | 1.37 | 0.9999 | 0.9999 | 0.0034 | 0.0034 | 0.9966 | 0.9966 |
| Test set 4 - 12 MHz | | | | | | | | | |
| 2.30 | 0.1660 | 1.40 | 1.40 | 0.9999 | 0.9999 | 0.8445 | 0.8445 | 0.1554 | 0.1554 |
| 18.5, 11.5 | 0.1575 | 8.30 | 14.6 | 0.9933 | 0.9793 | 0.0001 | 0.0001 | 0.9999 | 0.9999 |

**Table 4.** Ultrasound Characteristics for Various Tissue Lengths From Simulation- *(Continued)*

| Region thickness (mm) | Wavelength (mm) | Travel time (µs) | | Attenuation (Gain) | | Coefficients | | | |
|---|---|---|---|---|---|---|---|---|---|
| | | | | | | Reflection | | Transmission | |
| | | A | B | A | B | A | B | A | B |
| 11.0 | 0.3559 | 3.10 | - | 0.9714 | - | 0.2867 | - | 0.7133 | - |
| 0.57 | 0.1660 | 0.34 | 0.34 | 0.9999 | 0.9999 | 0.2804 | 0.0001 | 0.7196 | 0.9999 |
| 0.37 | 0.1524 | 0.24 | 0.24 | 0.9999 | 0.9999 | 0.0028 | 0.0028 | 0.9972 | 0.9972 |
| 2.50 | 0.1660 | 1.56 | 1.56 | 0.9999 | 0.9999 | 0.0028 | 0.0028 | 0.9972 | 0.9972 |
| Test set 5 - 12 MHz | | | | | | | | | |
| 2.60 | 0.1640 | 1.60 | 1.60 | 0.9999 | 0.9999 | 0.8461 | 0.8461 | 0.1539 | 0.1539 |
| 20.0, 12.0 | 0.1574 | 7.90 | 14.0 | 0.9938 | 0.9819 | 0.0001 | 0.0001 | 0.9999 | 0.9999 |
| 11.3 | 0.3646 | 3.10 | - | 0.9698 | - | 0.3064 | - | 0.6935 | - |
| 0.62 | 0.1640 | 0.38 | 0.38 | 0.9999 | 0.9999 | 0.3051 | 0.0001 | 0.6948 | 0.9999 |
| 0.39 | 0.15234 | 0.26 | 0.26 | 0.9999 | 0.9999 | 0.0021 | 0.0021 | 0.9978 | 0.9978 |
| 2.70 | 0.1640 | 1.65 | 1.65 | 0.9999 | 0.9999 | 0.0021 | 0.0021 | 0.9978 | 0.9978 |
| Test set 6 - 12 MHz | | | | | | | | | |
| 2.80 | 0.1620 | 1.73 | 1.73 | 0.9999 | 0.9999 | 0.8477 | 0.8477 | 0.1523 | 0.1523 |
| 21.5, 12.5 | 0.1572 | 7.63 | 12.72 | 0.9943 | 0.9843 | 0.0001 | 0.0001 | 0.9999 | 0.9999 |
| 11.7 | 0.3733 | 3.13 | - | 0.9676 | - | 0.3257 | - | 0.6743 | - |
| 0.70 | 0.1620 | 0.43 | 0.43 | 0.9999 | 0.9999 | 0.3293 | 0.0001 | 0.6706 | 0.9999 |
| 0.41 | 0.1523 | 0.27 | 0.27 | 0.9999 | 0.9999 | 0.0016 | 0.0016 | 0.9983 | 0.9983 |
| 2.80 | 0.1620 | 1.73 | 1.73 | 0.9999 | 0.9999 | 0.0016 | 0.0016 | 0.9983 | 0.9983 |
| Test set 7 - 15 MHz | | | | | | | | | |
| 3.10 | 0.1600 | 1.94 | 1.94 | 0.9998 | 0.9998 | 0.8493 | 0.8493 | 0.1510 | 0.1510 |
| 23.0, 13.0 | 0.1571 | 7.32 | 11.80 | 0.9948 | 0.9865 | 0.0001 | 0.0002 | 0.9998 | 0.9998 |
| 12.0 | 0.3820 | 3.14 | - | 0.9660 | - | 0.3441 | - | 0.6560 | - |
| 0.73 | 0.1600 | 0.46 | 0.46 | 0.9999 | 0.9999 | 0.3533 | 0.0002 | 0.6466 | 0.9998 |
| 0.43 | 0.1522 | 0.28 | 0.28 | 0.9999 | 0.9999 | 0.0012 | 0.0012 | 0.9988 | 0.9988 |
| 3.00 | 0.1600 | 1.90 | 1.90 | 0.9998 | 0.9998 | 0.0012 | 0.0012 | 0.9988 | 0.9988 |
| Test set 8 - 15 MHz | | | | | | | | | |
| 3.40 | 0.1580 | 2.15 | 2.15 | 0.9998 | 0.9998 | 0.8510 | 0.8510 | 0.1491 | 0.1491 |
| 24.5, 13.5 | 0.1569 | 7.01 | 10.83 | 0.9952 | 0.9886 | 0.0003 | 0.0003 | 0.9997 | 0.9997 |
| 12.3 | 0.3906 | 3.15 | - | 0.9643 | - | 0.3622 | - | 0.6377 | - |
| 0.80 | 0.1580 | 0.51 | 0.51 | 0.9999 | 0.9999 | 0.3765 | 0.0003 | 0.6234 | 0.9997 |
| 0.45 | 0.1521 | 0.30 | 0.30 | 0.9999 | 0.9999 | 0.0008 | 0.0008 | 0.9991 | 0.9991 |
| 3.20 | 0.1580 | 2.02 | 2.02 | 0.9998 | 0.9998 | 0.0008 | 0.0008 | 0.9991 | 0.9991 |
| Test set 9 - 15 MHz | | | | | | | | | |
| 3.70 | 0.1560 | 2.37 | 2.37 | 0.9998 | 0.9998 | 0.8525 | 0.8525 | 0.1475 | 0.1475 |
| 26.0, 14.0 | 0.1568 | 6.70 | 9.88 | 0.9956 | 0.9905 | 0.0007 | 0.0007 | 0.9993 | 0.9993 |
| 12.7 | 0.3993 | 3.18 | - | 0.9620 | - | 0.3799 | - | 0.6200 | - |
| 0.84 | 0.1560 | 0.54 | 0.54 | 0.9999 | 0.9999 | 0.3994 | 0.0007 | 0.6005 | 0.9993 |
| 0.48 | 0.1520 | 0.32 | 0.32 | 0.9999 | 0.9999 | 0.0005 | 0.0005 | 0.9995 | 0.9995 |
| 3.30 | 0.1560 | 2.12 | 2.12 | 0.9998 | 0.9998 | 0.0005 | 0.0005 | 0.9995 | 0.9995 |
| Test set 10 - 15 MHz | | | | | | | | | |

**Table 4.** Ultrasound Characteristics for Various Tissue Lengths From Simulation- *(Continued)*

| Region thickness (mm) | Wavelength (mm) | Travel time (μs) | | Attenuation (Gain) | | Coefficients | | | |
|---|---|---|---|---|---|---|---|---|---|
| | | | | | | Reflection | | Transmission | |
| | | A | B | A | B | A | B | A | B |
| 4.00 | 0.1540 | 2.60 | 2.60 | 0.9998 | 0.9998 | 0.8539 | 0.8539 | 0.1460 | 0.1460 |
| 27.5, 14.5 | 0.1566 | 6.40 | 8.94 | 0.9960 | 0.9923 | 0.0010 | 0.0010 | 0.9989 | 0.9989 |
| 13.0 | 0.4080 | 3.20 | - | 0.9602 | - | 0.3971 | - | 0.6029 | - |
| 0.90 | 0.1540 | 0.58 | 0.58 | 0.9999 | 0.9999 | 0.4215 | 0.4215 | 0.5785 | 0.9989 |
| 0.50 | 0.1519 | 0.33 | 0.33 | 0.9999 | 0.9999 | 0.0003 | 0.0003 | 0.9997 | 0.9997 |
| 3.50 | 0.1540 | 2.27 | 2.27 | 0.9998 | 0.9998 | 0.0003 | 0.0003 | 0.9997 | 0.9997 |

frequency for the design of the low pass filter for acquiring the shift frequencies was set to 1 MHz. The system was then tested with four different ICP pulses shown in Figure 18 (i.e. normal, normal challenging, abnormal and abnormal challenging ICP pulses) [2, 3]. The scope plots for major nodes in the SIMULINK simulation can be seen in Figure 17.

From the filtered multiplexed signal, FFT in MATLAB was used to identify the shift frequency for the received ultrasound pulse. This shift frequency was then used to calculate the instantaneous flow rate of the CSF (i.e. velocity). The found flow rate was then used to calculate the pressure within CSF (i.e. ICP). The original ICP signal and final received ICP signal can be seen in Figure 19. The ICP pulse was achieved with a variance of 63.62 Pa from the reference model used. This was due to the calculation of phase shift using FFT function and the recalculation of frequency shift value using the same function in MATLAB. The FFT function used introduced a small variance in the phase shift value.

The proposed device from the simulation can be developed for clinical use. From the design, patients will not experience discomfort or pain associated with non-invasive methods of ICP monitoring. Patients also gain the ability of mobility while using the proposed ICP monitoring device due to the wireless technology included in the design. Concerning the heating of the biological tissues, the use of short ultrasound pulses (0.5 μs) and large intervals (80 μs) allow for safe loss of heat due to ultrasound signal attenuation. Healthcare personnel also gain an easy to use and direct method for ICP monitoring in health centers. An MEMS ultrasound sensor can be used in the design of the sensor circuit to be attached to the human neck region [30, 31]. The small size and transducer arrays can aid in acquiring better signals. Note that this research covered the use of a single ultrasound transducer. Further work can be done to identify the effect of using an array of ultrasound transducers. The frequency of ultrasound device to be used can be maintained at 15 MHz for all ages. Wireless transmission was also not simulated in this work due to the extensive research and efficient existing wireless transmission systems/components. The computing system can be a little challenging to develop. This challenge will be due to the identification of the ultrasound receive pulses from the CSF contents (cells within). This was easier to implement in simulation but very difficult in circuit design. The main driving principle behind this device is the CSF content (cells within) and ultrasound signal interaction. To increase the probability of ultrasound-cells interaction, 80 μs pulse interval was used instead of larger values. The simulations run for this research was computationally intensive. This was due to the large number of model com-

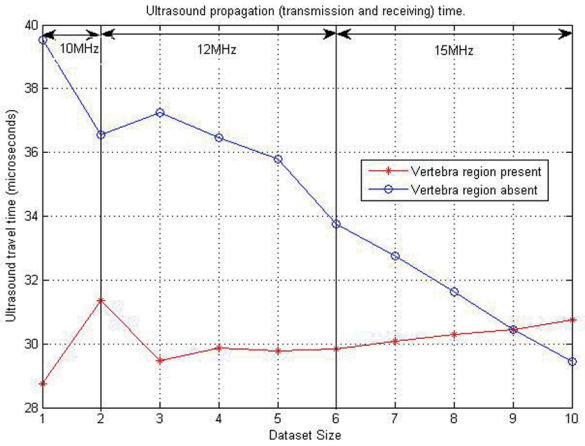


**Figure 15.** Ultrasound propagation time plot for various datasets considered.

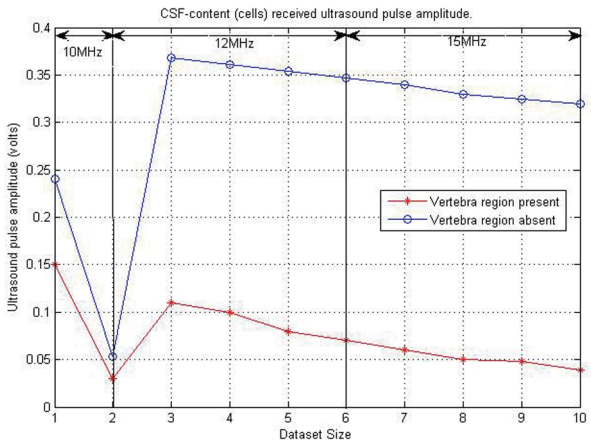


**Figure 16.** Graph showing CSF content and ultrasound pulse interaction received amplitude.

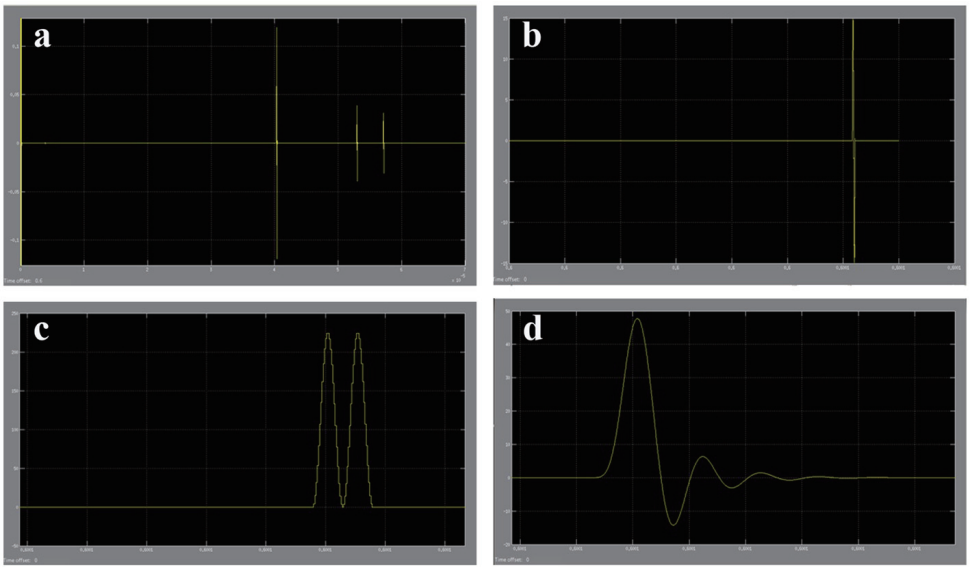


**Figure 17.** (a) Part of ultrasound pulses received from the SIMULINK biological system model. (b) Amplified received ultrasound pulse from CSF cells reflections. (c) The multiplexed signal of the original ultrasound pulse and the received amplified ultrasound pulse. (d) The filtered shifted ultrasound pulse (shift frequency) to remove high frequencies.

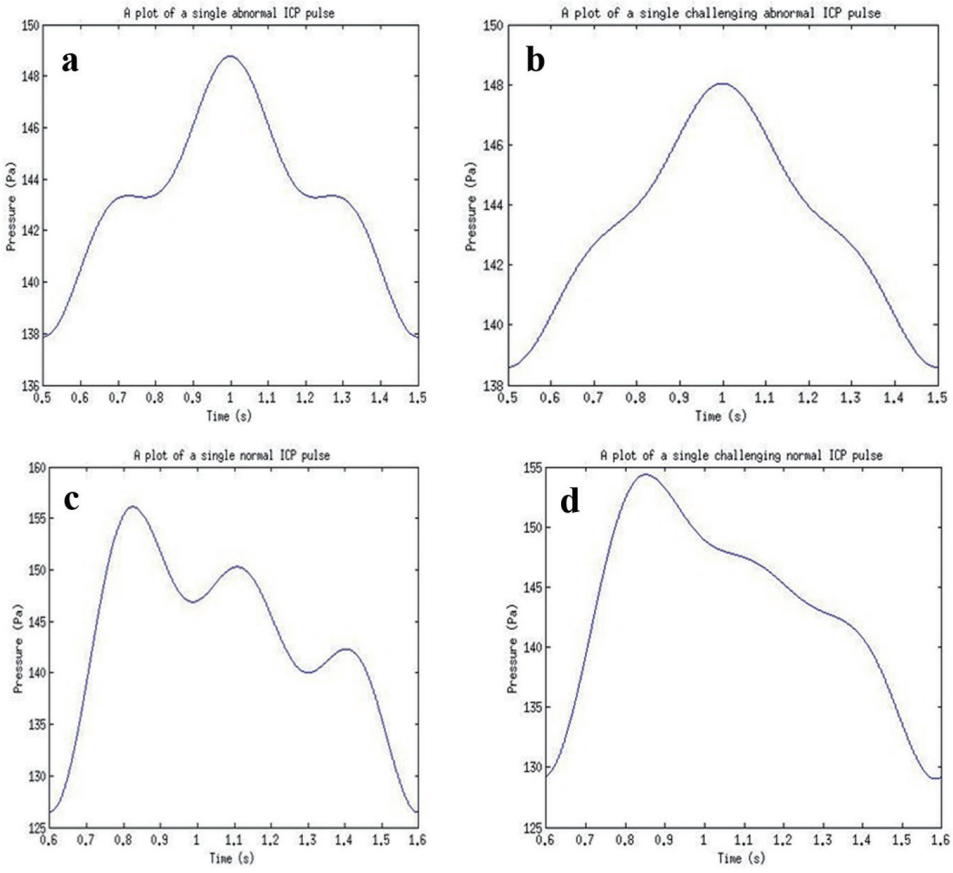


**Figure 18.** ICP pulses used for simulations for (a) an abnormal ICP pulse, (b) an abnormal challenging ICP pulse, (c) a normal ICP pulse, and (d) a normal challenging ICP pulse.

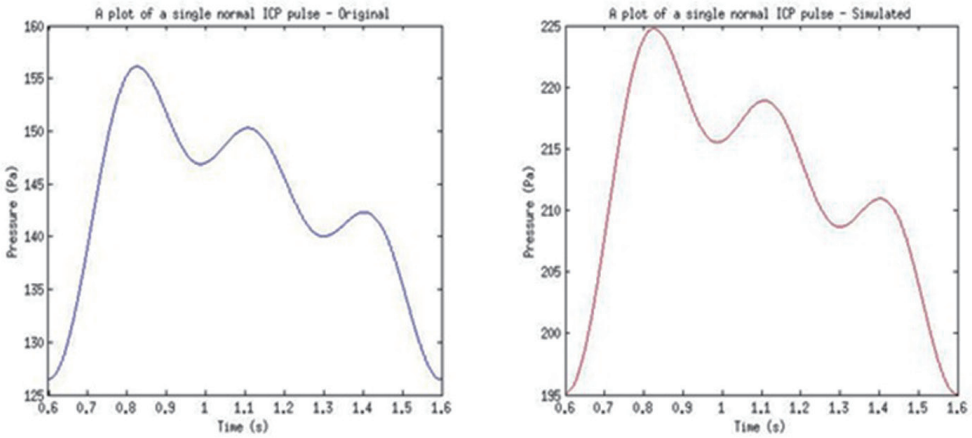


**Figure 19.** Example of results from the used of normal pulse in simulation.

ponents embedded in the SIMULINK model.

**Conclusion**

The present study establishes a reference model for ultrasound system-biological system interaction. The study also proposes a new approach for ICP monitoring. The proposed ultrasound ICP monitoring method was studied numerically using MATLAB and SIMULINK. The governing equations used were derived from ultrasound principles and Doppler theory. The model was applied to 10 different datasets and four ICP waveforms. The range of data used consisted of varying densities, speed of sound and tissue thickness. The appropriate minimum frequency for the proposed method is 10 MHz. The minimum pulse interval is 80 μs for on effective detection of shifted ultrasound pulse. The pulse generator low pass filter value used was 40 MHz. With the signal processing system filter, a 1 MHz low pass filter was used. The two systems designed work well with the appropriate data and the variables are easy to change. The dataset, results and behavior of the system correlate with both ultrasound principles and other studies done in this area. The proposed approach has the advantage of being an easy to use, non-invasive and a direct method for ICP monitoring. The proposed model from the discussed design will satisfy both the need of the patient and healthcare personnel. The model presented is an effective tool in the field of research, coursework and presentations.

## Acknowledgement

This research was supported by the research fund of Hanbat National University in 2012, the National Research Foundation of Korea (NRF) funded by the Ministry of Science, ICT & Future Planning (NRF-2013R1A1A1060503 & NRF-2014K1A3A1A09063284), and University of Ghana and the Carnegie Corporation of New York through UG-Carnegie Next Generation of Academics in Africa Scholarship 2013.

## Disclaimers

The views shared in this article are solely those of the authors.

## Sources of Support

UG-Carnegie Next Generation of Academics in Africa Scholarship and the research fund of Hanbat National University in 2013.

## Conflict of Interest

The authors declare they have no conflict of interests.

## Abbreviations

ρ: density; c: speed of sound; λ: wavelength of sound; α: attenuation coefficient of a particular tissue; RC: reflection coefficient of a particular tissue; TC: transmission coefficient of a particular tissue; $z_1$: acoustic impedance of the previous biological tissue; $z_2$: acoustic impedance of the current biological tissue; $f_o$: transmission frequency; $f_1$: received frequency; $f_d$: Doppler shift frequency; $A_o$: original amplitude of ultrasound wave before transmission; $A_i$: new amplitude of ultrasound wave after transmission; d: diameter of ultrasound transducer; r: radius of ultrasound transducer; v: velocity of CSF; P: pressure; $v_1$: peak flow velocity; $\mu_0$: mean ICP; $\mu_1$: fundamental harmonics of ICP signal; $\mu_2$: first harmonics of ICP signal; $\mu_3$: second harmonics of ICP signal; $\Theta_h$: phase of the first and second harmonics; $f_c$: ICP rate

## References

1. Kashif MF, Verghese GC, Novak V, Czosnyka M, Heldt

T. Model-Based Non-invasive Estimation of Intracranial Pressure from Cerebral Blood Flow Velocity and Arterial Pressure. Sci Transl Med. 2012;4(129):44.
2. McNames J, Goldstein B, Aboy M. Automatic Detection Algorithm of intracrainal pressure waveform components. IEEE Eng Med Biol Soc. 2001;3:2231-2234.
3. Scalzo F, Asgari S, Kim S, Bergsneider M, Hu X. Robust peak recognition in intracranial pressure signals. Biomed Eng Online. 2010;9:61.
4. Zhong J, Dujovny M, Park HK, Perez E, Perlin AR, Diaz FG. Advances in ICP monitoring techniques. Neurol Res. 2003;25(4):339-350.
5. Rosenberg JB, Shiloh AL, Savel RH, Eisen LA. Non-invasive methods of estimating intracranial pressure. Neurocrit Care. 2011;15(3):599-608.
6. Jackrit S, Sattayasoonthorn P. A Review of Development for Intracranial Pressure Measurement. In Proceedings of the 7th Asian Conference on Computer-Aided Surgery (ACCAS 2011), Bangkok, Thailand, 2011.
7. Newman WD, Hollman AS, Dutton GN, Carachi R. Measurement of optic nerve sheath diameter by ultrasound: a means of detecting acute raised intracranial pressure in hydrocephalus. Br J Ophthalmol. 2002;86(10):1109-1113.
8. Asiedu PD, Lee K, Mills G, Kaufmann EE. A review of Non-invasive Methods of Monitoring Intracranial Pressure. J Neurol Res. 2014;4(1):1-6.
9. Wakeland W, Goldstein B. A review of physiological simulation models of intracranial pressure dynamics. Comput Biol Med. 2008;38(9):1024-1041.
10. Heidi HK, Noble VE. Commentary Using MRI of the optic nerve shealth to detect elevated intracranial pressure. Crit Care. 2008:181.
11. Chan V, Perlas A, Narouze SN. Atlas of Ultrasound-Guided Procedures in Interventional Pain Management. Springer Sci Bus Media LLC. 2011:13-19,
12. Hendee WR, Ritenour ER. Medical Imaging Physics. Wiley-Liss Inc. 2002;4:304-353.
13. O'Brien WD Jr. Review Ultrasound - biophysics mechanisms. Elsevier. 2007.
14. Abbaszadeh J, Rahim HA, Rahim RA, Sarafi S, Ayob MN, Faramarzi M. Design procedure of ultrasonic tomography system with steel pipe conveyor. Sens Actuators 203 Elsevier BV. 2013:215-224,.
15. Bushberg JT, Leidholdt EM, Boone JM, Seibert JA. The Essential Physics of Medical Imaging, 2nd ed. Philadelphia, USA: lippincott Williams and Wilkins. 2002.
16. Aboy M, McNames J, Homero R, Thong T, Cuesta D, Goldstein B. A novel statistical Model for Simulation of Arterial and intracranial Pressure. Proc 26th Annu Int Conf IEEE EMBS. 2004:129-132.
17. Forouzanfar M, Balasingam B, Dajani HR, Groza VZ, Bolic M, Rajan S, Petriu EM. Mathematical Modeling and Parameter Estimation of Blood Pressure Oscillometric Waveform. IEEE. 2012:1-6.
18. Bjorsell J, Ferm Lithem V, Torma J. Simulation model of an ultrasonicsensor used in non-destructivetesting. Uppsala University, Uppsala, Sweden. 2013.
19. Hillard J, Arroyo MD, Case M. Ultrasound Blood flow Sensing using Doppler Velocimetry. Int J Smart Sens Intell Syst. 2013;6(4):1298-1316.
20. Azhari T. Basics of Biomedical Ultrasound for Engineers. John Wiley and Sons Inc. 2010.
21. Hendriks FM. Mechanical Behaviour of Human Skin in Vivo, A Literature Review. K Philips Electron NV. 2001:23-39.
22. Kayelaby. Medical ultrasonics. Acoustics SubSection. 2014.
23. Zhang L, Chen HB, Wang Y, Zhang LY, Liu JC, Wang ZG. Cervical spinal canal narrowing and cervical neurological injuries. Chin J Traumatol. 2012;15(1):36-41.
24. Zhou JM, Cannata QF, Shung KK. Piezoelectric Materials for high frequency medical imaging applications: A review. J Electroceramics. 2007;19:139-145.
25. Hirsch LJ, Gibney MA, Albanese J, Qu S, Kassler-Taub K, Klaff LJ, Bailey TS. Comparative glycemic control, safety and patient ratings for a new 4 mm x 32G insulin pen needle in adults with diabetes. Curr Med Res Opin. 2010;26(6):1531-1541.
26. Gibney MA, Arce CH, Byron KJ, Hirsch LJ. Skin and subcutaneous adipose layer thickness in adults with diabetes at sites used for insulin injections: implications for needle length recommendations. Curr Med Res Opin. 2010;26(6):1519-1530.
27. Presti DL, Ingegnosi C, Strauss K. Skin and subcutaneous thickness at injecting sites in children with diabates: ultrasound findings and injecting recommendations. Pediatr Diabetes. 2012;13:1-9.
28. Cambier D, D'Herde K, Witvrouw E, Beck M, Soenens S, Vanderstraeten G. Therapeutic ultrasound: temperature increase at different depths by different modes in a human cadaver. J Rehabil Med. 2001;33(5):212-215.
29. Saladin K. Anatomy and Physiology: The Unity of Form and Function, 5th ed. McGraw Hill Primis. 2009.
30. Satyanarayana T, Srinivas G, Srinivas Prasad MVVK, Srinivas Y, Sudheer B, Srinivas a Rao K. Design and Analysis of MEMS based Composite Piezoelectric Ultrasound transducer. Electr Electron Eng. 2012;2(6):362-373.
31. Pattnaik P, Jena J, Pradhan SK, Kamilla SK, Mohanty MN. Design of Ultrasonic Transducer MEMS Model for Distance Measurement using Multiphysics. Int J Adv Comput Res. 2013;3(8)215-219.

 